molecules

MDPI

Article

First-Principles Study of Atomic Diffusion by Vacancy Defect of the $L1_2$-Al_3M (M = Sc, Zr, Er, Y) Phase

Shuai Liu [1], Binbin Liao [1], Baohua Nie [1,*], Touwen Fan [2], Dongchu Chen [1], Jianglong Zhang [3] and Yu Song [4,*]

[1] School of Materials Science and Hydrogen Energy, Foshan University, Foshan 528000, China; chendc@fosu.edu.cn (D.C.)
[2] Research Institute of Automobile Parts Technology, Hunan Institute of Technology, Hengyang 421002, China
[3] Shenyuan Honors of College, Beihang University, Beijing 100191, China
[4] Shenzhen Rspower Technology Co., Ltd., Shenzhen 518000, China
* Correspondence: niebaohua@fosu.edu.cn (B.N.); songyu188200@foxmail.com (Y.S.); Tel.: +86-757-8270-0525 (B.N.); +86-755-8323-3458 (Y.S.)

Abstract: Atomic diffusion by the vacancy defect of $L1_2$-Al_3M (M = Sc, Zr, Er, Y) was investigated based on a first-principles calculation. The point defect formation energies were firstly evaluated. Then, the migration energy for different diffusion paths was obtained by the climbing-image nudged elastic band (CI-NEB) method. The results showed that Al atomic and M atomic diffusions through nearest-neighbor jump (NNJ) mediated by Al vacancy (V_{Al}) were, respectively, the preferred diffusion paths in Al_3M phases under both Al-rich and M-rich conditions. The other mechanisms, such as six-jump cycle (6JC) and next-nearest-neighbor jump (NNNJ), were energetically inhibited. The order of activation barriers for NNJ(Al-V_{Al}) was Al_3Zr < Al_3Y < Al_3Er < Al_3Sc. The Al_3Sc phase had high stability with a high self-diffusion activation barrier, while the Al_3Zr and Al_3Y phases were relatively unstable with a low self-diffusion activation energy. Moreover, the atomic-diffusion behavior between the core and shell layers of $L1_2$-Al_3M was also further investigated. Zr atoms were prone to diffusion into the Al_3Y core layer, resulting in no stable core-shelled Al_3(Y,Zr), which well agreed with experimental observation.

Keywords: first-principles calculation; vacancy defect; atomic diffusion; $L1_2$-Al_3M

Citation: Liu, S.; Liao, B.; Nie, B.; Fan, T.; Chen, D.; Zhang, J.; Song, Y. First-Principles Study of Atomic Diffusion by Vacancy Defect of the $L1_2$-Al_3M (M = Sc, Zr, Er, Y) Phase. *Molecules* **2023**, *28*, 6727. https://doi.org/10.3390/molecules28186727

Received: 17 August 2023
Revised: 4 September 2023
Accepted: 13 September 2023
Published: 21 September 2023

1. Introduction

Aluminum alloys containing transition metals (TM) and rare-earth (RE) elements are widely used in aerospace, high-speed trains, and automobiles [1–3]. The formation of $L1_2$-Al_3(RE,TM) nanophases with high thermal stability, such as the core-shelled Al_3(Sc,Zr) nanophase, can effectively inhibit the recrystallization process of aluminum alloys, achieving high strength toughness and corrosion resistance performance [2]. Based on the high thermostability and coarsening resistance of $L1_2$-Al_3(RE,TM) nanophases, Seidman et al. [4–6] developed an Al-RE-TM series of high-temperature aluminum alloys.

Due to the high cost of Sc elements, low-cost elements that can form thermally stable Al_3M phases were explored to replace Sc elements. A first-principles calculation showed that Er and Yb elements were candidate element to replace Sc elements [7,8]. The Zr element can partially replace Sc element and was considered an ideal element to form the Al_3Zr shell structure owing to the Al_3Zr/Al interface with low interface energy and coherent strain energy [9]. The typical core-shelled nanophases, such as Al_3(Er,Zr) [10] and Al_3(Yb,Zr) [11], were introduced in aluminum alloys to replace Al_3(Sc,Zr) nanophases. The formation of these core-shelled Al_3M phases was explained by the difference in diffusion rates between elements, that is, the rapid diffusion elements were enriched to form a core layer and the slow diffusion elements were segregated to form a shell layer [12]. The core-double-shelled structure that was observed in Al-Sc-Er-Zr alloys contained an Er-enriched core surrounded by a Sc-enriched core and a Zr-enriched outer shell, obtaining a high coarsening resistant

and high strength [5,13]. The formation of the core-double-shelled structure well agreed with the prediction by the atomic diffusivity ordering of $D_{Er} > D_{Sc} > D_{Zr,}$

The Y element, as a Sc homologous element with similar physical and chemical properties, was a probable candidate element to replace the Sc element [14]. Zhang et al. [15,16] showed that core-shelled Al_3(Y,Zr) with a Y-rich core and Zr-rich shell can be formed during the early stage of aging in Al-Y-Zr alloys. The Al_3Y phase acted as the heterogeneous core to accelerate the precipitation of Al_3Zr, which well agreed with the atomic-diffusion control mechanism. However, atom probe tomography (APT) showed that Y and Zr atoms were randomly distributed in the $L1_2$-Al_3(Y,Zr), and hybrid structure, rather than core-shelled structure, was observed in the Al_3(Y,Zr) phase after long-term aging. The strong binding energy between Y and Zr atoms was assumed to explain the formation of hybrid structure Al_3(Y,Zr) [16]. According to the authors' previous investigation, the core-shelled Al_3Y/Al_3Zr was thermodynamically unstable due to its high coherent strain energy of Al_3Y/Al_3Zr. A similar transition from a core-shelled structure to a hybrid structure during long-term aging was also observed in the Al-Yb-Sc alloy [17]. Seidman et al. [17] suggested that the inter-diffusion of Yb and Sc resulted in a uniform distribution of elements throughout the precipitates. Thus, the mechanism of the $L1_2$-Al_3M phase with core-shelled structure or hybrid structure needed to be answered.

Atomic diffusion, especially mediated by vacancy, was very beneficial for understanding the microstructural stability of the $L1_2$-Al_3M phase [18]. Although experimental methods were difficult to investigate atomic diffusion in intermetallic compounds [19,20], first-principles calculations can provide new insights into the microscopic mechanisms of atomic diffusion [18,20]. First-principles calculations by Fan [21,22] showed that with the increase of the atomic number, the diffusion rate of rare-earth elements increased from Sc to Y, La, and then decreased to Lu. Shi et al. [23] investigated the atomic diffusion of pure and transition-element (TM)-doped $L1_2$-Al_3Sc based on first principles and found that under a strong Al-rich condition, the V_{Sc} defect obtained low formation energy and the NNJ mechanism mediated by V_{Al} was most favorable for Sc atomic diffusion. TM dopants increased diffusion activation energy for dominant Al_3Sc diffusion. However, the atomic diffusion between the core layer and the shell layer for the core-shelled $L1_2$-Al_3M phase was far from fully understood.

The atomic-diffusion mechanism in the $L1_2$-Al_3M (M = Sc, Er, Y, Zr) phases was investigated based on the first-principles in the present work. The formation energy of point defects was calculated. Then, migration energy along possible diffusion was analyzed by the climbing-image nudged elastic band (CI-NEB) method [24]. Thus, the diffusion activation energy was obtained. Furthermore, the atomic-diffusion behavior between the core and shell layers for the core-shelled $L1_2$-Al_3M phase was also further illustrated. The purpose of this study was to reveal the microscopic mechanism of atomic diffusion in the $L1_2$-Al_3M phases and core-shelled $L1_2$-Al_3M phase, providing a theoretical guidance for the development of high-performance aluminum alloys containing TM and RE elements.

2. Results and Discussion

2.1. Defect Formation Energy

In order to evaluate the difficulty of point defect formation, the formation energy of point defects in Al_3M was calculated as [25]

$$E_f^{def} = E_{total}^{def} - E_{total}^{bulk} - \sum_i \Delta n_i \mu_i \quad (1)$$

Here, E_{total}^{def} and E_{total}^{bulk} are the total energy of the defective supercell and the total energy of the defect-free supercell, respectively. n_i represents the number of i atoms (i = Al or M) that increased ($\Delta n_i > 0$) or decreased ($\Delta n_i < 0$) when defects were formed, and μ_i is the relative chemical potential of i atoms.

To maintain a stably balanced $L1_2$ phase, its chemical potential should meet the following requirement:

$$3\Delta\mu_{Al} + \Delta\mu_M = \Delta H_f^{Al_3M} \quad (2)$$

Here, $\Delta H_f^{Al_3M}$ is the formation enthalpy of the unit chemical formula Al_3M in the solid state; $\Delta\mu_{Al}$ and $\Delta\mu_M$ are the differences between the relative chemical potentials of Al and M atoms, respectively, and the chemical potentials of solid simple substance, which can be expressed as

$$\begin{aligned} \Delta\mu_{Al} &= \mu_{Al} - \mu_{Al}^{bulk} \\ \Delta\mu_M &= \mu_M - \mu_M^{bulk} \end{aligned} \quad (3)$$

Here, μ_{Al}^{bulk} and μ_M^{bulk} are the chemical potentials of the metals Al and M, respectively, that is, the single-atomic energies in the elemental state.

In order to avoid the precipitation of the solid elements Al and M, the chemical potential of each atom in the defect phase should be less than that of the solid elements, that is,

$$\begin{aligned} \Delta\mu_{Al} &\leq 0 \\ \Delta\mu_M &\leq 0 \end{aligned} \quad (4)$$

From the phase diagram of each Al-M system, Al_3M was in equilibrium with the adjacent pure Al phase, as the non-stoichiometric ratio was Al-rich due to point defects. When the non-stoichiometric ratio was M-rich due to point defects, the Al_3M phase was in equilibrium with the adjacent stoichiometric Al_2M phase. In order to avoid the formation of the pure Al and Al_2M secondary phase, the chemical potential should be limited by the following:

$$\begin{aligned} &\Delta\mu_{Al} \leq 0 \\ &2\Delta\mu_{Al} + \Delta\mu_M \leq \Delta H_f^{Al_2M} \end{aligned} \quad (5)$$

Here, $\Delta H_f^{Al_2M}$ is the formation enthalpy of the unit chemical formula Al_2M in the solid state.

The formation energies of four kinds of defects in the $L1_2$-Al_3M phase were calculated, as shown in Figure 1. Under the Al-rich condition, the point defects of V_{Sc} obtained low formation energy and were the main point defects for the Al_3Sc phase, and the point defects of Al_{Er} and V_{Er} were the main point defects for the Al_3Er phase. The Sc_{Al} and Er_{Al} defects were the main point defects for the Al_3Sc phase and Al_3Er phase owing to the lowest formation energy under Sc-rich and Er-rich conditions. The point defects of the Al_3Sc phase under Al-rich and Sc-rich conditions were well consistent with Ref. [23]. On the other hand, the change of the stoichiometric ratio had little effect on the formation energy of the point defects in the Al_3Zr phase and Al_3Y phase. The V_{Zr} and Al_Y defects obtained the lowest formation energy for the Al_3Zr phase and Al_3Y phase regardless of the Al-rich, Zr-rich, and Y-rich conditions. Furthermore, the defect energy of V_{Zr} was a negative value, indicating that the Al_3Zr phase was inclined to form stable V_{Zr} vacancy defects under the Al-rich condition. The formation energy of the Y_{Al} antisite was always the highest; thus, it was difficult to form Y_{Al} antisite defects in the Al_3Y phase. Shi et al. [23] suggested that the point defect formation energy was dependent on the electronic structure and the value of the electronic density of state (DOS) at the Fermi level. However, V_{Al} was the primary point defect near the stoichiometry [23]. Similar vacancy defects were reported in the Ni_3Al phase [18], where vacancies defect on the Ni sublattice was the main point defect in the Ni_3Al phase.

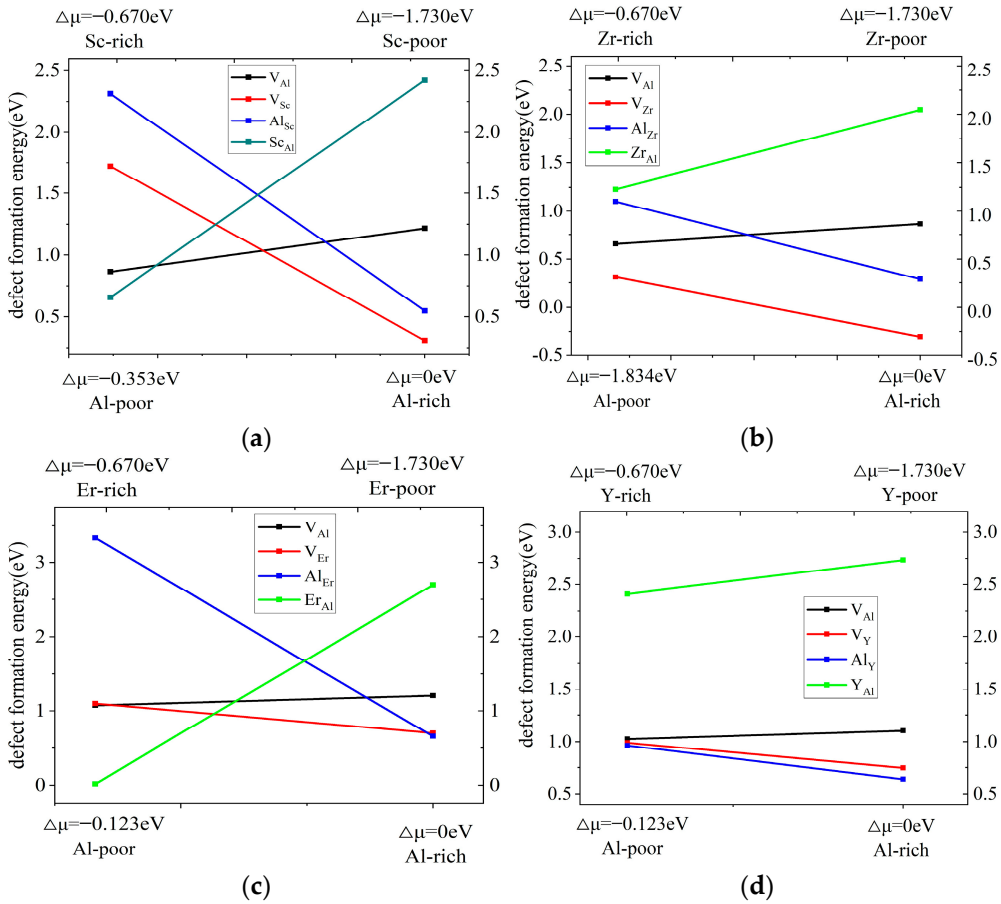

Figure 1. Formation energies of vacancy and antisite defects of $L1_2$-Al_3M phase: (**a**) Al_3Sc defect; (**b**) Al_3Zr defect; (**c**) Al_3Er defect; and (**d**) Al_3Y defect.

2.2. *Vacancy-Mediated Atomic Migration*

2.2.1. Al Atomic Migration

Figure 2a–c show the energy profiles for Al atomic diffusion mediated by V_{Al} in the Al_3M phase. The nearest-neighbor site Al around V_{Al} can migrate to V_{Al} through the symmetrical NNJ pathways (denoted as NNJ(Al-V_{Al})), and the energy profile was symmetrical due to the restoration of the local disordered structures (Figure 2a). The highest energies of the energy profile corresponding to the migration barrier were 0.913 eV, 0.914 eV, 0.647 eV, and 0.622 eV for Al_3Sc, Al_3Zr, Al_3Er, and Al_3Y, respectively, indicating that NNJ(Al-V_{Al}) with the low migration barrier was the preferred diffusion path for Al_3M phases owing to the direct jump to V_{Al}. Furthermore, the migration barrier of Al_3Sc was almost the same as that of Al_3Zr, while Al_3Er and Al_3Y obtained low migration barriers. The different migration barrier for the NNJ path can be attributed to the different M atomic sizes. The Er and Y atoms had large atomic radii; thus, the Al_3Er and Al_3Y obtained high lattice gaps, where Al atoms can migrate through the large atomic gaps to V_{Al}, obtaining a lower migration barrier.

Al atoms that occupied the next-nearest-neighbor sites of V_{Al} can migrate to V_{Al} through two types of diffusion paths, denoted as NNNJ1 and NNNJ2, as shown in Figure 2b,c. As for the NNNJ1 path, the order of migration energy was Al_3Zr > Al_3Sc > Al_3Er > Al_3Y. Al atoms migrated through the quadrangle composed of the nearest-neighbor Al atoms, where the quadrangle gap became large with the increase in M atomic radius; correspondingly, the migration energy decreased with the increase in M atomic radius. However, the migration energies of the NNNJ2 path were almost the same and significantly increased owing to the high density of the quadrangle with two Al atoms and two M atoms. Compared with the NNJ migration, the Al atoms through the NNNJ1 and NNNJ2 paths needed to cross the

quadrangle composed of four neighboring atoms, illustrating higher migration energy [23]. Therefore, the tendency of Al migration by NNNJ was very low.

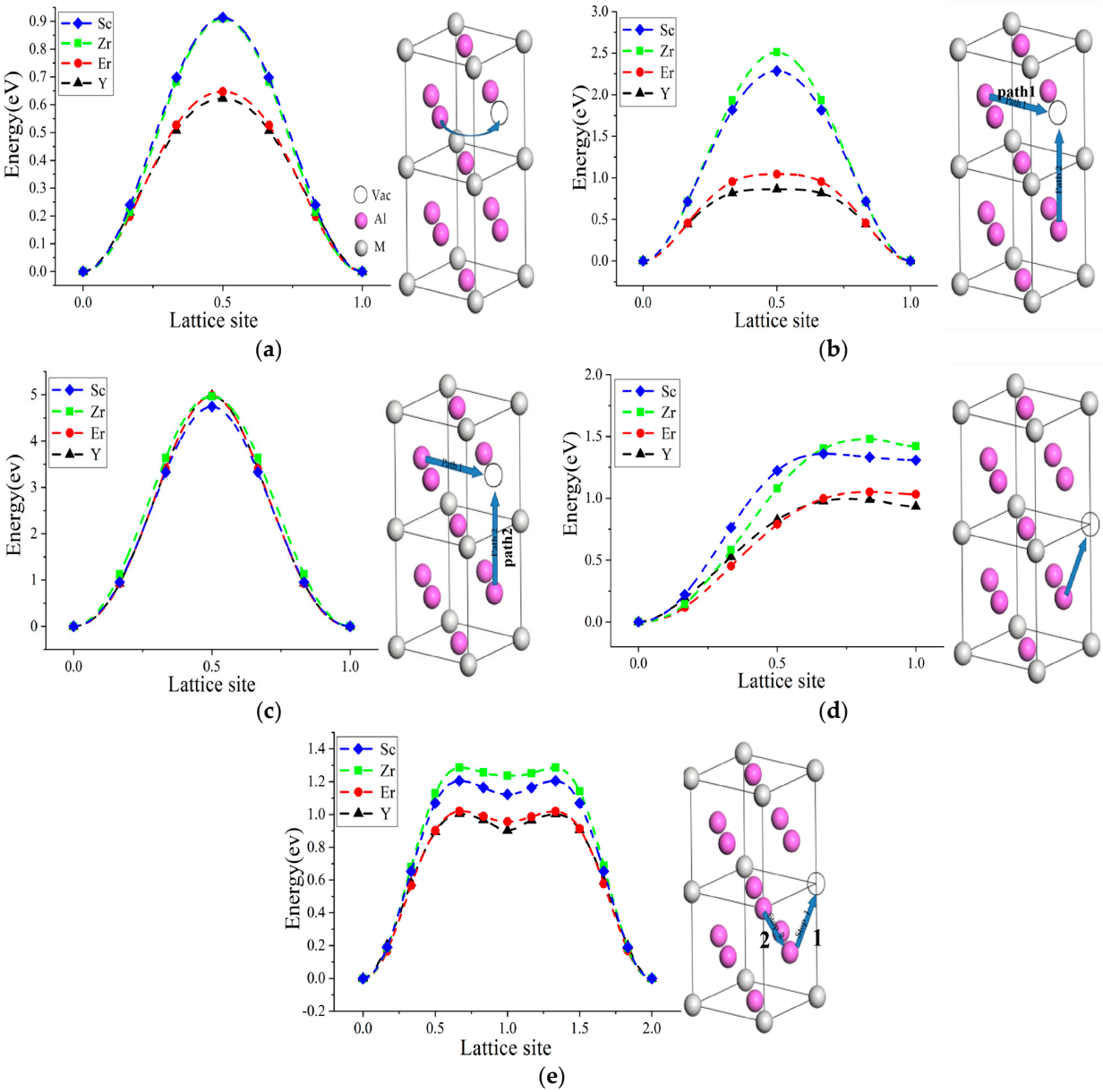

Figure 2. Energy profiles for Al atom diffusion in Al_3M phase: (**a**) NNJ(Al-V_{Al}); (**b**) NNNJ1(Al-V_{Al}); (**c**) NNNJ2(Al-V_{Al}); (**d**) NNJ(Al-V_M); and (**e**) ASB(Al_M-Al-V_M). The blue arrow represented the path of atomic jump.

The diffusion of Al atoms was also mediated by V_M, including the NNJ and ASB migration paths. Figure 2d shows the migration-energy profile for the NNJ path of Al atom mediated by V_M (denoted as NNJ(Al-V_M)), where the migration barriers mediated by V_M were still higher than that by V_{Al}. Meanwhile, the final state of migration was unstable due to the local disorder by the migration of Al atoms to V_M. In this sense, NNJ(Al-V_M) was not the preferred migration path. As for the ASB migration (Figure 2e), Al_M occupied the next-nearest-neighbor site of V_M, and the nearest-neighbor Al atoms migrated to V_M, forming V_{Al} (step 1). Then, Al_M migrated to the newly formed V_{Al} (step 2), denoted as ASB(Al_M-Al-V_M). The order of migration energy for AS and ASB was similar to that for NNNJ1 as Al_3Zr > Al_3Sc > Al_3Er > Al_3Y, which can be explained by the different M atomic radii. Although the disorder of the migration final state was restored to the migration

initial state, the ASB migration of Al atoms mediated by V_M was restricted due to the higher migration barrier of the NNJ migration by V_{Al}. From the above discussion, the NNJ(Al-V_{Al}) path had the lowest migration energy and was the main migration pathway for Al atomic migration.

2.2.2. M Atomic Migration

The migration of M atoms mediated by V_{Al} included the NNJ, AS, ASB, and 6JC paths. The migration of the nearest-neighbor M atoms jumped to V_{Al}, denoted as NNJ(M-V_{Al}), as shown in Figure 3a. The migration barriers of NNJ(M-V_{Al}) were far higher than that of NNJ(Al-V_{Al}). Meanwhile, the final state of migration was unstable due to the local disorder with the formation of M_{Al} and V_M defects. However, the Y atoms needed to overcome the increasing energy barrier during the migration process, suggesting that this migration path of Y atoms was energetically prohibited.

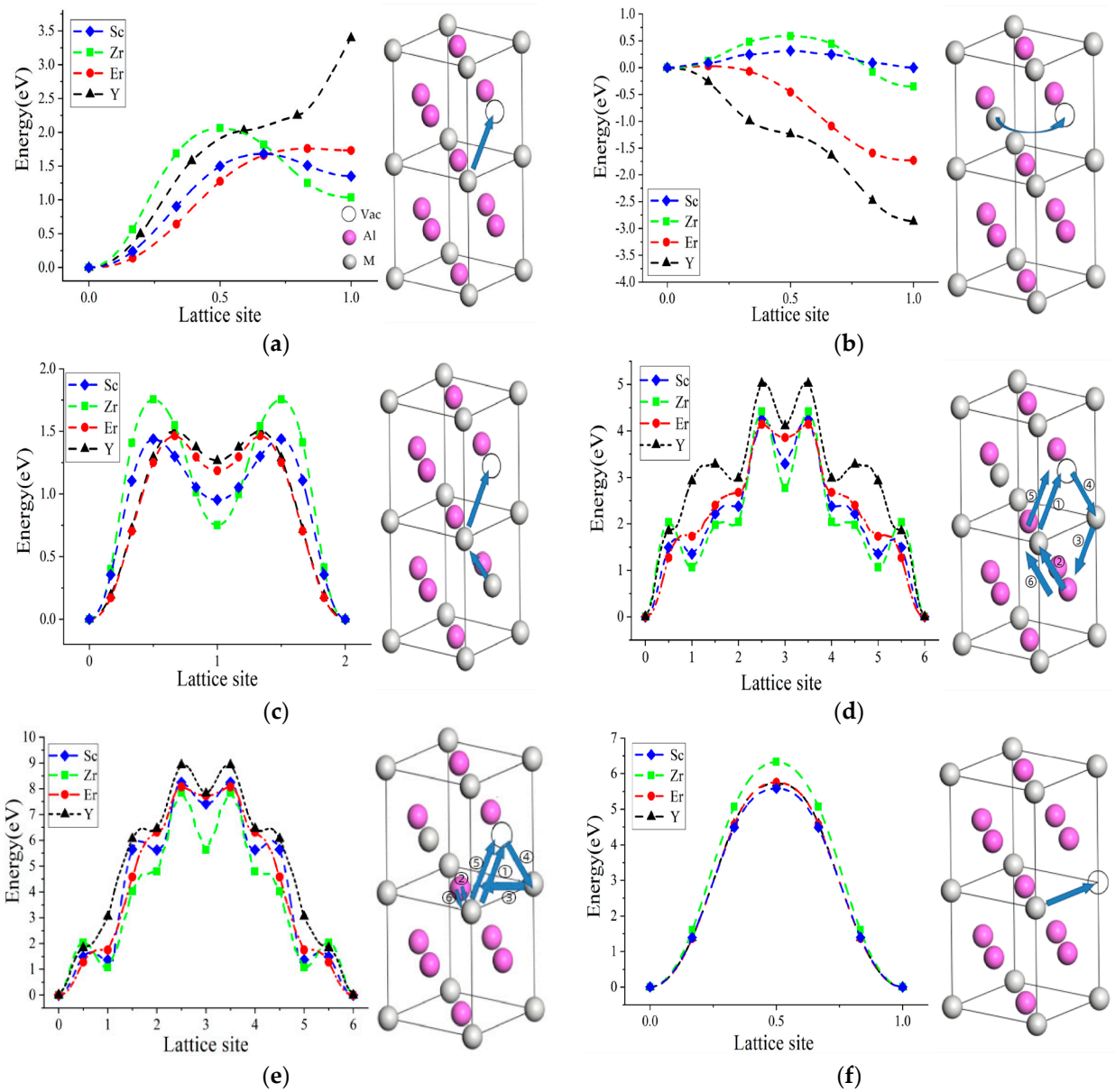

Figure 3. Energy profiles for M (M = Sc, Zr, Er, Y) atomic diffusion in Al_3M phase: (**a**) NNJ(M-V_{Al}); (**b**) AS(M_{Al}-V_{Al}); (**c**) ASB(M_{Al}-M-V_{Al}); (**d**) straight 6JC; (**e**) bent 6JC; and (**f**) NNNJ(M-V_M). The blue arrow represented the path of atomic jump.

The AS migration path was another M diffusion path, where the M_{Al} atoms directly migrated to V_{Al} (denoted as AS(M_{Al}-V_{Al})), as shown in Figure 3b. The migration barriers of the AS(M_{Al}-V_{Al}) path were very low compared with that of NNJ(M-V_{Al}). Except for the Al_3Sc phase, the final state energies of the Al_3Zr, Al_3Er, and Al_3Y phases were negative, which was inconsistent with the fact that the local disorder restored to their initial state after M atomic migration. It suggested that the AS(M_{Al}-V_{Al}) path did not exist for the Al_3Zr, Al_3Er, and Al_3Y phases in terms of energy. Furthermore, the AS(Sc_{Al}-V_{Al}) migration path was limited to some extent due to the difficulty of coexisting V_{Al} and Sc_{Al} in nearby locations.

For the ASB migration path, M_{Al} atoms and V_{Al} occupied the site of Al atoms (Figure 3c). The nearest-neighbor M firstly jumped to V_{Al}, newly forming a V_M and M_{Al} atom; then, the M_{Al} atom migrated to the new V_M vacancy, resulting in a V_{Al} (denoted as ASB(M_{Al}-M-V_{Al})). Obviously, the local disorder of the final state was consistent with that of the initial state; therefore, the migration-energy curve of the M atoms was symmetric. These two migration steps corresponded to the two saddle-curve characteristics of M atomic-migration energy. The Zr atomic migration by the ASB path in the Al_3Zr phase obtained the maximum migration energy with 1.754 eV, which was lower than that of NNJ(M-V_{Al}) with 2.059 eV. Meanwhile, the migration barriers of the Er, Y, and Sc atoms were nearly the same for the ASB path. However, the ASB pathway was limited due to the simultaneous presence of both M_{Al} and V_{Al} defects.

The 6JC path of M atomic migration mediated by V_{Al} consisted of the straight 6JC path and the bent 6JC path, as shown in Figure 3d,e. The six steps in the straight 6JC and bent 6JC were described in detail in Ref. [23]. The energy curves of M diffusion by straight 6JC and bent 6JC were symmetric due to the restoration of local disorder after the six-step migration process. The first step (M-V_{Al}) in the straight 6JC and bent 6JC paths was similar to that of NNJ(M-V_{Al}). In the first step, the migration energy of the Y atom increased during the migration process, while the migration energy of the Sc and Zr elements decreased after the migration to V_{Al}. Thus, the Y atomic diffusion obtained far higher migration energy than the Er, Sc, and Zr atoms. The high migration barriers for the Y, Er, Sc, and Zr atoms indicated the straight 6JC and bent 6JC paths were energetically restricted.

The migration of M atoms mediated by V_M is also shown in Figure 3f. The M atom at the next-nearest-neighbor site jumped to V_M (denoted as NNNJ(M-V_M)), and the energy profile of the M diffusion was symmetric owing to the restoration of local disorder. The Zr atom obtained the higher migration barrier than that of the Er, Sc, and Y atoms due to the dense structure of the Al_3Zr phase. However, the Sc atomic diffusion had the lowest migration barrier, which did not agree with the effect of atomic size. Therefore, the migration barrier was related not only to the atomic radius of M but also to the electronic structure of the M atom [23]. Furthermore, the migration barriers of M atoms for NNNJ(M-V_M) were much higher than that for NNJ(M-V_{Al}) and ASB(M_{Al}-M-V_{Al}), suggesting that the NNNJ(M-V_M) migration path was not a preferred migration path.

From the above discussion, except the AS(Sc_{Al}-V_{Al}) path being the preferred path for Sc atomic migration, the NNJ(M-V_{Al}) and ASB(M_{Al}-M-V_{Al}) paths contributed to M atomic migration, while the straight 6JC, bent 6JC, and NNNJ(M-V_M) paths were energetically prohibited.

2.3. Diffusion Activation Barrier

In the process of vacancy-mediated atomic diffusion, the activation barrier had a decisive influence on atomic diffusion and can be expressed as [23]:

$$\Delta E_a = \Delta E_f^{defect} + \Delta E_m \quad (6)$$

Here, ΔE_f^{defect} is the defect formation energy of the initial state, and ΔE_m is the migration barrier for different migration paths.

Table 1 shows that the calculated diffusion activation energies of the Al and M atoms in the Al_3M phases. The calculation of the Al_3Sc phase generally agreed with that of Ref. [23].

Under the Al-rich condition, the Al atomic-diffusion activation barriers of NNJ(Al-V_M) were lower than that of NNJ(Al-V_{Al}) in the Al_3M phases, which was attributed to the low V_M formation energies under the Al-rich condition. However, the diffusion path of NNJ(Al-V_M) was restricted due to the unstable final state (Figure 2d). Thus, NNJ(Al-V_{Al}) diffusion was the main diffusion path for Al atoms under both Al-rich and M-rich conditions.

Table 1. Diffusion activation barrier of $L1_2$-Al_3M.

System	Diffusion Atoms	Diffusion Mechanisms	Activation Barrier (eV)	
			Al-Rich	Sc-Rich
Al_3Sc	Al	NNJ(Al-V_{Al})	2.131–2.250 [23]	1.778–1.689 [23]
		NNJ(Al-V_{Sc})	1.668–2.352 [23]	3.081–3.916 [23]
		NNNJ1(Al-V_{Al})	3.503–3.825 [23]	3.150–3.244 [23]
		NNNJ2(Al-V_{Al})	5.963–6.441 [23]	5.609–5.860 [23]
		ASB(Al_{Sc}-Al-V_{Sc})	2.346–2.628 [23]	5.574–6.297 [23]
	Sc	NNJ(Sc-V_{Al})	2.900–3.124 [23]	2.547–2.543 [23]
		AS(Sc_{Al}-V_{Al})	3.956–4.144 [23]	1.178–1.148 [23]
		ASB(Sc_{Al}-Sc-V_{Al})	5.079–5.546 [23]	2.958–2.640 [23]
		NNNJ(Sc-V_{Sc})	5.893–8.881 [23]	7.306–10.625 [23]
		S6JC(Sc----V_{Al})	5.489–4.759 [23]	5.135–6.504 [23]
		B6JC(Sc----V_{Al})	9.430–10.154 [23]	9.076–10.734 [23]
Al_3Zr	Al	NNJ(Al-V_{Al})	1.776	1.572
		NNJ(Al-V_{Zr})	1.175	1.788
		NNNJ1(Al-V_{Al})	3.376	3.172
		NNNJ2(Al-V_{Al})	6.183	5.830
		ASB(Al_{Zr}-Al-V_{Zr})	1.736	3.166
	Zr	NNJ(Zr-V_{Al})	2.926	2.721
		AS(Zr_{Al}-V_{Al})	-	-
		ASB(Zr_{Al}-Zr-V_{Al})	4.666	3.645
		NNNJ(Zr-V_{Zr})	6.029	6.642
		S6JC(Zr----V_{Al})	5.373	5.169
		B6JC(Zr----V_{Al})	8.755	8.550
Al_3Er	Al	NNJ(Al-V_{Al})	1.856	1.722
		NNJ(Al-V_{Er})	1.748	2.149
		NNNJ1(Al-V_{Al})	1.969	1.888
		NNNJ2(Al-V_{Al})	6.187	6.053
		ASB(Al_{Er}-Al-V_{Er})	2.849	5.932
	Er	NNJ(Er-V_{Al})	2.966	2.832
		AS(Er_{Al}-V_{Al})	-	-
		ASB(Er_{Al}-Er-V_{Al})	5.370	2.555
		NNNJ(Er-V_{Zr})	6.451	6.853
		S6JC(Er----V_{Al})	5.350	5.216
		B6JC(Er----V_{Al})	9.220	9.086
Al_3Y	Al	NNJ(Al-V_{Al})	1.730	1.649
		NNJ(Al-V_Y)	1.725	1.968
		NNNJ1(Al-V_{Al})	1.969	1.888
		NNNJ2(Al-V_{Al})	6.090	6.009
		ASB(Al_Y-Al-V_Y)	2.885	3.452
	Y	NNJ(Y-V_{Al})	4.507	4.426
		AS(Y_{Al}-V_{Al})	-	-
		ASB(Y_{Al}-Y-V_{Al})	5.347	4.942
		NNNJ(Y-V_{Sc})	6.472	6.715
		S6JC(Y----V_{Al})	6.203	6.172
		B6JC(Y----V_{Al})	10.230	10.149

For M atomic diffusion, NNJ(M-V_{Al}) diffusion obtained the low activation barriers for the Sc, Zr, Er, and Y atoms under both Al-rich and M-rich conditions, thus becoming the

energetically preferred diffusion path. The diffusion activation barriers of Y atoms were far higher than that of the Sc, Zr, and Er elements due to their large atomic radii. Although the diffusion barriers of AS(Sc_{Al}-V_{Al}) and ASB(Er_{Al}-Er-V_{Al}) were much lower under the M-rich condition, their contribution to Sc atomic and Er atomic diffusions was limited due to the difficulty of coexisting V_{Al} and Sc_{Al}, Er_{Al} defects in nearby locations.

The activation barriers of Al atomic and M atomic diffusions mediated by V_{Al} under the M-rich condition were generally lower than that under the Al-rich condition owing to the lower formation energy of V_{Al}. The diffusion activation barriers of Al atoms in the Al_3M phase were lower than that of M atoms. Moreover, ASB, NNNJ, straight 6JC, and bent 6JC mechanisms with high diffusion activation barriers were not factually executed for Al atomic and M atomic diffusions under both Al-rich and M-rich conditions. Therefore, the NNJ(Al-V_{Al}) diffusion under the M-rich condition was the most preferred diffusion mechanism in the Al_3M phase, and the order of activation barriers was Al_3Zr < Al_3Y < Al_3Er < Al_3Sc. It should be noted that these calculations were Al-atomic-self-diffusion activation barriers in the Al_3M phase. It implied that the Al_3Sc phase had high stability with a high self-diffusion activation energy, while the Al_3Zr phase was relatively unstable with a low self-diffusion activation barrier, which well agreed with the fact that the Al_3Zr phase transformed from the $L1_2$ structure to $D0_{23}$ structure at high temperatures [26].

2.4. Atomic Diffusion of Core-Shelled $L1_2$-Al_3(N,Zr)

The addition of the Er, Y, Sc, and Zr elements in aluminum alloys typically formed $L1_2$-Al_3M phases with a core-shelled structure. Due to the low interface energy between the Al_3Zr phase and aluminum matrix, the Al_3Zr phase tended to form a shell layer, and the Al_3N (N = Sc, Er, Y) phase was inclined to form a core layer, where the core-shell structure was denoted as Al_3(N,Zr). Atomic diffusion between the Al_3N core and Al_3Zr shell was investigated in this section. The Zr atomic diffusion to the Al_3N core and the N atomic diffusion to the Al_3Zr shell were respectively calculated. The previous investigation showed that Zr atoms in the Al_3Zr shell reciprocally substituted the site of N atoms in the Al_3N core [27].

As described in Section 2.3, NNJ(M-V_{Al}) was the preferred diffusion path for Zr atoms in the Al_3N core, where Zr atoms occupied the site of N atoms at the nearest-neighbor site of V_{Al}. The formation energy of V_{Al} was affected by Zr atomic substitution and can be expressed as

$$E_f^{def}(Zr_N) = E_{total}^{def}(Zr_N) - E_{total}^{bulk} - \sum_i \Delta n_i \mu_i - \mu_{Zr} \quad (7)$$

Here, $E_{total}^{def}(Zr_N)$ is the total energy of defective supercell with Zr substitution. μ_{Zr} is the chemical potential of Zr atoms.

For the N atomic substitution for Zr atoms in the Al_3Zr shell, the formation energies of V_{Al} defect with N atomic substitution are expressed as

$$E_f^{def}(N_{Zr}) = E_{total}^{def}(N_{Zr}) - E_{total}^{bulk} - \sum_i \Delta n_i \mu_i - \mu_N \quad (8)$$

Here, $E_{total}^{def}(N_{Zr})$ is the total energy of the defective supercell with N substitution. μ_N is the chemical potential of N atoms.

Table 2 shows that the formation energy of the V_{Al} defect with Zr substitution was within that of the pure Al_3N phase between Al-rich and N-rich, and Zr substitution had little influence on the formation energy of the V_{Al} defect due to the atomic radius of Al being close to that of Zr. As shown in Table 3, the Sc substitution for Zr atoms slightly increased the formation energy of the V_{Al} defect, while the Er and Y substitutions significantly increased the formation energy of the V_{Al} defect.

Table 2. Formation energy of V_{Al} defect in pure and Zr-substituted Al_3N core.

	Formation Energy of V_{Al} (eV)		
	Al_3Sc	**Al_3Er**	**Al_3Y**
Pure	0.863–1.217	1.074–1.208	1.026–1.107
Zr substitution	1.194	1.187	1.063

Table 3. Formation energy of V_{Al} defect in pure and N-substituted Al_3Zr shell.

	Pure	**Sc**	**Er**	**Y**
V_{Al} (eV)	0.661–0.865	0.884	1.136	1.359

Zr atoms were considered to migrate through the NNJ path mediated by V_{Al} in the Al_3N core, as shown in Figure 4a. The migration barriers of Zr diffusion in the Al_3Sc, Al_3Er, and Al_3Y cores were 1.658 eV, 1.653 eV, and 1.570 eV, respectively, which were far lower than that in the Al_3Zr phase with 2.059 eV. The order of migration barriers for Zr atoms in the Al_3N core was Al_3Sc > Al_3Er >Al_3Y. With the increase in the N atomic radius for the Al_3N core, Zr atoms easily migrated due to the increase in the lattice gap. Thus, Zr atomic diffusion in the Al_3Y core obtained the lowest migration energy. Figure 4b illustrates that the diffusion of Sc, Er, and Y atoms in the Al_3Zr shell obtained migration barriers with 2.14 eV, 2.356 eV, and 2.53 eV, respectively, which were higher than that of Zr migration in the Al_3Zr shell with 2.059 eV. The atomic-migration energy in the Al_3Zr shell was sequentially Y > Er > Sc, which can be attributed to the high diffusion resistance for the large atomic radius.

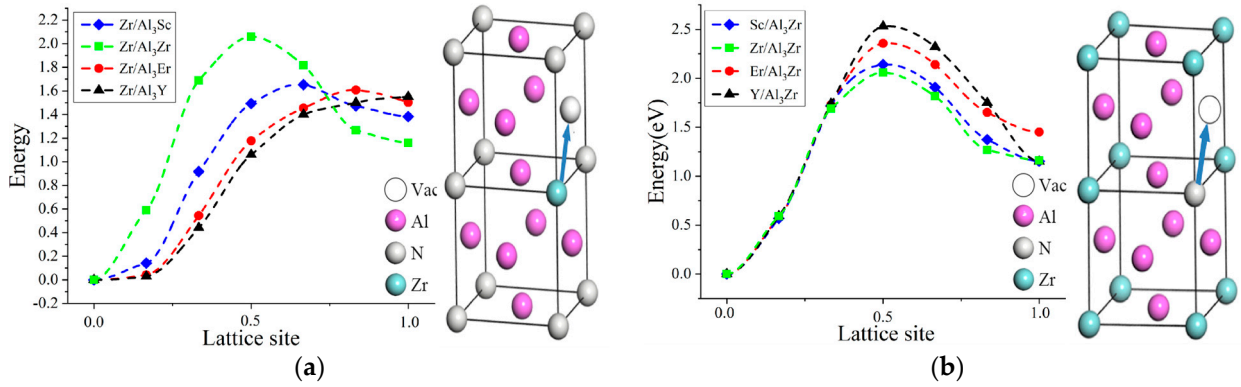

Figure 4. Atomic-migration energy of core-shelled $L1_2$-Al_3Zr(N): (**a**) the migration of Zr atom of Al_3Zr shell layer to core Al_3N phase and (**b**) the migration of N atom of Al_3N core layer to shell Al_3Zr phase. The blue arrow represented the path of atomic jump.

As the diffusion activation barrier included vacancy formation energy and atomic-migration energy, the diffusion activation energies of Zr atoms in the Al_3Sc, Al_3Er, and Al_3Y cores were 2.852 eV, 2.84 eV, and 2.633 eV, respectively. Additionally, the diffusion activation barriers of the Sc, Er, and Y atoms in the Al_3Zr shell were 3.024 eV, 3.492 eV, and 3.889 eV, respectively. Compared with the diffusions of the Sc, Er, and Y atoms into the Al_3Zr shell, Zr atoms were more inclined to enter the $A_{l3}Sc$, Al_3Er, and Al_3Y cores based on diffusion activation energy. Furthermore, Zr atoms preferred to diffuse into the Al_3Y core, while the diffusion of Zr atoms into the Al_3Er and Al_3Sc cores required higher activation barriers. It revealed that Zr atoms in the Al_3Zr shell were inclined to diffuse into the Al_3Y core during the subsequent aging process, thus resulting in no typical core-shelled structure. However, Zr atoms were difficult to diffuse into Al_3Sc and Al_3Er cores due to their high diffusion activation barrier, thus maintaining a typical core-shelled structure.

3. Computational Methods

Based on density functional theory (DFT) [28], first-principles calculations were carried out by Vienna ab initio simulation package (VASP) software [29]. The projector augmented wave (PAW) with the Perdew–Burke–Ernzerh (PBE) method of generalized gradient approximation (GGA) was used to describe the exchange-correlation energy functional between electrons [30]. The electron configuration was described by the Al-$3s^2 3p^1$, Sc-$3s^2 3p^6 4s^1 3d^2$, Zr-$4s^2 4p^6 5s^1 4d^3$, Er-$6s^2 5p^6 5d^1$, and Y-$4s^2 4p^6 5s^1 4d^2$ valence states, respectively. The kinetic energy cutoff of the plane-wave basis and the size of the k-mesh for the Brillouin zone were tested for self-consistent convergence. The geometric structure was optimized by the Monkhorst-Pack k-point grids with linear k-mesh analytical values of less than 0.032π/Å. The total energy was calculated using the linear tetrahedron method with the Blöchl correction when the total energy converged to 10^{-4} eV/atom. The lattice constants (a_0) were predicted as 4.042 Å, 4.103 Å, 4.108 Å, and 4.232 Å for fcc-Al, $L1_2$-Al_3Sc, $L1_2$-Al_3Zr, and $L1_2$-Al_3Er, respectively, which were well consistent with Ref. [31].

There were two sublattices in the $L1_2$-Al_3M (M = Sc, Zr, Er, Y) unit cell, the Al sublattice located at the 3c position (0,0.5,0.5) and the M sublattice located at the 1a (position (0,0,0). Therefore, there were four types of primary point defects in Al_3M, including Al vacancy (V_{Al}), M vacancy (V_M), Al antisite (Al_M), and M antisite (M_{Al}). In order to reduce vacancy density and limit the interaction between defects, 108 atoms in a 3 × 3 × 3 supercell were used in this calculation.

The diffusion mechanism of the $L1_2$-Al_3M phase mediated by vacancy included from the nearest-neighbor to complex hopping sequences, such as nearest-neighbor jump (NNJ), next-nearest-neighbor jump (NNNJ), antistructural sublattice (AS), antistructural bridge (ASB), and 6-jump cycle (6JC) [23]. The CI-NEB method [24] was used to calculate the energy profile. A series of atomic positions were inserted between the initial and final states to construct the model, and then, each insertion point model was relaxed until the force threshold at the insertion point was 10^{-2} eV/Å. By this method, the vacancy diffusion behavior of the $L1_2$-Al_3M phase was comparatively studied, and the atomic-diffusion interaction between the core layer and the shell layer for the core-shelled $L1_2$-Al_3M phase was also discussed.

4. Conclusions

Atomic-diffusion mechanisms in $L1_2$-Al_3M (M = Sc, Er, Y, Zr) phases were investigated based on a first-principles calculation. The main conclusions are summarized as follows:

(1) NNJ(Al-V_{Al}) and NNJ(M-V_{Al}) diffusions were the energetically preferred diffusion paths under both Al-rich and M-rich conditions. The straight 6JC, bent 6JC, and NNNJ were significantly inhibited owing to their high activation barriers. Other diffusion paths, such as NNJ(Al-V_M), AS(Sc_{Al}-V_{Al}), and ASB(Er_{Al}-Er-V_{Al}), were limited due to the unstable final-state structure and the difficulty of coexisting V_{Al} and M_{Al} defects.

(2) The order of activation barriers for NNJ(Al-V_{Al}) was Al_3Zr < Al_3Y < Al_3Er < Al_3Sc. The Al_3Sc phase had high stability with a high self-diffusion activation barrier, while the Al_3Zr phase was relatively unstable with a low self-diffusion activation energy.

(3) Compared with the diffusion of the Sc, Er, and Y atoms in the Al_3Zr shell, Zr atoms were more inclined to diffuse into the Al_3Y, Al_3Er, and Al_3Sc cores, and the activation barriers were as follows: Al_3Y < Al_3Er < Al_3Sc. Thus, Zr atoms were prone to diffuse into the Al_3Y core, resulting in no core-shelled structure.

Author Contributions: B.N. and Y.S. conceived and designed the research; S.L., B.L. and J.Z. performed the first-principles calculation; T.F. and D.C. analyzed the experimental data; S.L. wrote the manuscript. All authors have read and agreed to the published version of the manuscript.

Funding: This research was funded by the R & D plan for key areas in Guangdong Province (2020B010186001), Science and Technology Program of the Ministry of Science and Technology (G2022030060L), Science and technology project in Guangdong (2020b15120093, 2020B121202002), Overseas famous teacher project of Guangdong(BGK46303), Science and technology research project

of Foshan (2220001005305), and R and D plan for key areas in Jiangxi Province (20201BBE51009, 20212BBE51012).

Data Availability Statement: The data presented in this study are available on request from the corresponding author.

Conflicts of Interest: The authors declare no conflict of interest.

Sample Availability: Not applicable.

References

1. Dursun, T.; Soutis, C. Recent developments in advanced aircraft aluminium alloys. *Mater. Des.* **2014**, *56*, 862–871. [CrossRef]
2. Ye, J.; Pan, Q.; Liu, B.; Hu, Q.; Qu, L.; Wang, W.; Wang, X. Effects of co-addition of minor Sc and Zr on aging precipitates and mechanical properties of Al-Zn-Mg-Cu alloys. *J. Mater. Res. Technol.* **2023**, *22*, 2944–2954. [CrossRef]
3. Deng, P.; Mo, W.; Ouyang, Z.; Tang, C.; Luo, B.; Bai, Z. Mechanical properties and corrosion behaviors of (Sc, Zr) modified Al-Cu-Mg alloy. *Mater. Charact.* **2022**, *196*, 112619. [CrossRef]
4. De Luca, A.; Seidman, D.N.; Dunand, D.C. Effects of Mo and Mn microadditions on strengthening and over-homogenization resistance of nanoprecipitation-strengthened Al-Zr-Sc-Er-Si alloys. *Acta Mater.* **2019**, *165*, 1–14. [CrossRef]
5. Booth-Morrison, C.; Dunand, D.C.; Seidman, D.N. Coarsening resistance at 400 °C of precipitation-strengthened Al-Zr-Sc-Er alloys. *Acta Mater.* **2011**, *59*, 7029–7042. [CrossRef]
6. Farkoosh, A.R.; Dunand, D.C.; Seidman, D.N. Effects of W and Si microadditions on microstructure and the strength of dilute precipitation-strengthened Al-Zr-Er alloys. *Mater. Sci. Eng. A* **2020**, *798*, 140159. [CrossRef]
7. Liu, S.; Liu, F.; Yan, Z.; Nie, B.; Fan, T.; Chen, D.; Song, Y. Nucleation of $L1_2$-Al_3M (M = Sc, Er, Y, Zr) Nanophases in Aluminum Alloys: A First-Principles Thermodynamics Study. *Crystals* **2023**, *13*, 1228. [CrossRef]
8. Lan, J.; Chen, Z.; Liu, L.; Zhang, Q.; He, M.; Li, J.; Peng, X.; Fan, T. The Thermal Properties of $L1_2$ Phases in Aluminum Enhanced by Alloying Elements. *Metals* **2021**, *11*, 1420. [CrossRef]
9. Song, Y.; Zhan, S.; Nie, B.; Liu, S.; Qi, H.; Liu, F.; Fan, T.; Chen, D. First-principle investigation of the interface properties of the core-shelled $L1_2$-Al_3M (M = Sc, Zr, Er, Y) Phase. *Crystals* **2023**, *13*, 420. [CrossRef]
10. Xue, D.; Wei, W.; Wen, S.; Wu, X.; Shi, W.; Zhou, X.; Gao, K.; Huang, H.; Nie, Z. Microstructural evolution of Al-Mg-Er-Zr alloy by equal channel angular extrusion at room temperature. *Mater. Lett.* **2023**, *334*, 133759. [CrossRef]
11. Peng, G.; Chen, K.; Fang, H.; Chen, S. A study of nanoscale Al_3 (Zr, Yb) dispersoids structure and thermal stability in Al-Zr-Yb alloy. *Mater. Sci. Eng. A* **2012**, *535*, 311–315. [CrossRef]
12. Clouet, E.; Laé, L.; Épicier, T.; Lefebvre, W.; Nastar, M.; Deschamps, A. Complex precipitation pathways in multicomponent alloys. *Nat. Mater.* **2006**, *5*, 482–488. [CrossRef] [PubMed]
13. Chen, S.; Li, C.; Lian, G.; Guo, C.; Du, Z. Effect of elastic strain energy on the core-shell structures of the precipitates in Al-Sc-Er alloys. *J. Rare Earths* **2012**, *30*, 1276–1280. [CrossRef]
14. Zhang, X.D.; Wang, S.Q. First-principles study of thermodynamic properties and solubility of aluminum-rare-earth intermetallics. *Comput. Mater. Sci.* **2014**, *90*, 56. [CrossRef]
15. Zhang, Y.; Gu, J.; Tian, Y.; Gao, H.; Wang, J.; Sun, B. Microstructural evolution and mechanical property of Al-Zr and Al-Zr-Y alloys. *Mater. Sci. Eng. A* **2014**, *616*, 132–140. [CrossRef]
16. Gao, H.; Feng, W.; Wang, Y.; Gu, J.; Zhang, Y.; Wang, J.; Sun, B. Structural and compositional evolution of Al_3(Zr, Y) precipitates in Al-Zr-Y alloy. *Mater. Charact.* **2016**, *121*, 195–198. [CrossRef]
17. Van Dalen, M.E.; Dunand, D.C.; Seidman, D.N. Microstructural evolution and creep properties of precipitation-strengthened Al-0.06 Sc-0.02 Gd and Al-0.06 Sc-0.02 Yb (at.%) alloys. *Acta Mater.* **2011**, *59*, 5224–5237. [CrossRef]
18. Zhang, X.; Wang, C.Y. First-principles study of vacancy formation and migration in clean and Re-doped γ'-Ni_3Al. *Acta Mater.* **2009**, *57*, 224–231. [CrossRef]
19. Yan, K.; Chen, Z.W.; Zhao, Y.N.; Ren, C.C.; Aldeen, A.W. Morphological characteristics of Al_3Sc particles and crystallographic orientation relationships of Al_3Sc/Al interface in cast Al-Sc alloy. *J. Alloys Compd.* **2020**, *861*, 158491. [CrossRef]
20. Li, S.-S.; Li, L.; Han, J.; Wang, C.T.; Xiao, Y.Q.; Jian, X.D.; Qian, P.; Su, Y.J. First-Principles study on the nucleation of precipitates in ternary Al alloys doped with Sc, Li, Zr, and Ti elements. *Appl. Surf. Sci.* **2020**, *526*, 146455. [CrossRef]
21. Hu, T.; Ruan, Z.; Fan, T.; Wang, K.; He, K.; Wu, Y. First-principles investigation of the diffusion of TM and the nucleation and growth of $L1_2$-Al_3TM particles in Al alloys. *Crystals* **2023**, *13*, 1032. [CrossRef]
22. Fan, T.; Ruan, Z.; Zhong, F.; Xie, C.; Li, X.; Chen, D.; Tang, P.; Wu, Y. Nucleation and growth of $L1_2$-Al_3RE particles in aluminum alloys: A first-principles study. *J. Rare Earths* **2023**, *41*, 1116–1126. [CrossRef]
23. Shi, T.T.; Wang, J.N.; Wang, Y.P.; Wang, H.C.; Tang, B.Y. Atomic diffusion mediated by vacancy defects in pure and transition element (TM)-doped (TM = Ti, Y, Zr or Hf) $L1_2$-Al_3Sc. *Mater. Des.* **2016**, *108*, 529–537. [CrossRef]
24. Henkelman, G.; Uberuaga, B.P.; Jónsson, H. A climbing image nudged elastic band method for finding saddle points and minimum energy paths. *J. Chem. Phys.* **2000**, *113*, 9901–9904. [CrossRef]
25. Schmidt, C.; Bocquet, J. Calculation of the diffusion parameters in an ordered Ni_3Alalloy for a relaxed lattice. *Proc. Mater. Res. Soc.* **1998**, *527*, 165–170. [CrossRef]

26. Pan, S.; Li, C.; Qian, F.; Hao, L.; Li, Y. Diffusion controlled early-stage $L1_2$-$D0_{23}$ transitions within Al_3Zr. *Scr. Mater.* **2023**, *231*, 115460. [CrossRef]
27. Zhang, C.; Jiang, Y.; Cao, F.; Hu, T.; Wang, Y.; Yin, D. Formation of coherent, core-shelled nano-particles in dilute Al-Sc-Zr alloys from the first-principles. *J. Mater. Sci. Technol.* **2019**, *35*, 930–938. [CrossRef]
28. Nityananda, R.; Hohenberg, P.; Kohn, W. Inhomogeneous electron gas. *Resonance* **2017**, *22*, 809–811. [CrossRef]
29. Kresse, G.; Furthmüller, J. Efficiency of ab-initio total energy calculations for metals and semiconductors using a plane-wave basis set. *Comp. Mater. Sci.* **1996**, *6*, 15–50. [CrossRef]
30. Kresse, G.; Joubert, D. From ultrasoft pseudopotentials to the projector augmented-wave method. *Phys. Rev. B* **1999**, *59*, 1758–1775. [CrossRef]
31. Liu, X.; Wang, Q.; Zhao, C.; Li, H.; Wang, M.; Chen, D.; Wang, H. Formation of ordered precipitates in Al-Sc-Er-(Si/Zr) alloy from first-principles study. *J. Rare Earths* **2023**, *9*, 609–620. [CrossRef]